Mechanisms of strain localization and nucleation of earthquake faulting by grain-scale processes at the middle crustal level

Chunru. Hou[1], Junlai. Liu[1†], Yuanyuan. Zheng[1], Yanqi. Sun[1], Tieying. Zhang[1]， Baojun. Zhou[1], Wenkui, Fan[1]

[1]State Key Laboratory of Geological processes and mineral resources, China University of Geosciences, Beijing 100083, China.

Corresponding author: Junlai. Liu ([†]jliu@cugb.edu.cn)

Key Points:

- Microcracks at the tips of biotite drive fluids migration during initial deformation.
- Biotite grains play a leading role in strain localization.
- Strain localization zones are preludes to earthquakes faulting at the base of BDT.

Abstract

Understanding the mechanisms of strain localization is the key to our understanding of the transition from steady-state flow to unstable flow in the middle crust. In this paper, studies on deformation of gneisses sheared at mid-crustal level along the Jinzhou detachment fault zone, Liaodong peninsula, North China, reveal that biotite grains, as pre-existing weak-phase, have important influences on deformation of middle-crustal rocks. High phase strength contrasts between biotite grains and other mineral phases resulted in stress concentrations during shearing and occurrences of microcracks at the tips of biotite grains. Consequently, microcracks are formed either along contacts between high strength mineral grains or propagate into the mineral grains. The microcracks filled with biotite grains and fine-grained feldspar aggregates continue to nucleate, propagate, and coalesce in the rocks, while basal plane slip and grain boundary sliding (GBS) operate in biotite grains and fine-grained feldspar aggregates, respectively. These processes lead to a transition from load-bearing framework (i.e., coarse plagioclase grains) to interconnected weak phase (i.e., biotite grains and fine-grained feldspar aggregates), and the formation of incipient strain localization zones (SLZs). With the propagation and linkage of the SLZs, high stress concentrations at the tips of SLZs lead to nucleation of fractures. At the same time, there occurs an abrupt increase in strain rates that result in the transition from dislocation creep and GBS (velocity strengthening) to unstable slip (velocity weakening). The processes are accompanied by occurrence of mid-crustal earthquakes, and formation of pseudotachylite veins along with SLZs.

1 Introduction

Continental middle crust is a critical layer of the globe to our understanding of intracontinental tectonic processes, orogenic belts evolution, and seismogenic mechanisms (especially catastrophic earthquakes) (e.g., Lin et al., 2005; Lopez-Sanchez & Llana-Fúneza, 2018; Niemeijer & Spiers, 2007). The rheological behavior of middle-crustal rocks is characterized by coexisting brittle-ductile transition processes that are closely related to strain localization (e.g., Lin et al., 2005; Stewart & Miranda, 2017; White, 1996; White, 2012). The genetic relationships between brittle-ductile transition and strain localization, however, are still an enigma due to complicated governing factors, especially, the environmental parameters, e.g., temperatures, pressures, fluids and strain rates during natural deformation of the continental crust. Meanwhile, the compositions and fabrics of the rocks, e.g., the mineral phases and their relative proportion, and the structural characteristics at grain-scale, also have profound impacts on their rheological behaviors. Combining with experimental studies, theoretical calculations, and numerical simulations, detailed studies of exhumed crustal shear zones will help understand the rheological controls on the deformation of middle crustal rocks (e.g., Sibson, 1975; Fusseis et al., 2009; Price et al., 2012).

Strain localization occurs in zones of low rheological strength. Studies of weakening of rocks, and nucleation, propagation, and coalescence of strain localization zones (SLZs) are of profound significance to our knowledge on the initiation and evolution of crustal-scale faults, and to our understanding of intraplate deformation and plate tectonic processes (e.g., Platt & Behr, 2011). The increase of mica content and interconnection of mica grains in the rocks, and the transition from grain size insensitive creep (GSI) to grain size sensitive creep (GSS) of feldspar and quartz due to grain-size reduction were considered to be the most important mechanisms for strain weakening and strain localization at the middle crust (e.g., Fukuda &

Okudaira, 2013; Gueydan & Frédéric, 2003; Mansard et al., 2018; Oliot et al., 2014; Wibberley, 1999; Wintsch et al., 1995; Wintsch & Yeh, 2013). These mechanisms and processes lead to the transition from load-bearing framework (LBF) to interconnected weak phase (IWP). However, how this transition is accomplished at the middle crust remains hotly debated. Some studies suggested that pre-existing anisotropic interfaces are in favor of this transition, such as the pre-existing failure or lithological interfaces (e.g., Christiansen & Pollard, 1997; Guermani & Pennacchioni, 1998; Ingles et al., 1999; Pennacchioni, 2005; Pennacchioni & Mancktelow, 2007; Segall & Simpson, 1986; Wehrems et al, 2017). The interfaces tend to have lower rheological strength, and provide channels for fluids migration with reaction softening. Even microcracks generated during deformation may also promote the transition (e.g., Goncalves et al., 2016; Fusseis & Handy, 2008); Evolving rock fabrics during deformation provide other possibilities, e.g., transformation of mineral phases from feldspar to mica, grain size reduction of feldspar or quartz grains by subgrain rotation recrystallization (SGR), bulging recrystallization (BLG), or fragmentation accompanying the operation of GSS (e.g., Lucas, 1990; Oliot et al., 2014; Czaplińska et al., 2015). These processes cause strain weakening and generate interconnected weak-zones during deformation. In addition, an often less concerned problem is the changes in widths of SLZs after their formation. Previous studies addressed that the SLZs may be widened due to strain hardening. For example, deforming minerals may interlock with each other (e.g., Whitmeyer & Wintsch, 2005), or fluids are expelled outwards due to high pressure in shear zone, which dries the grain boundaries and impeding the occurrence of GBS (e.g., Finch et al., 2016). Besides, chemical potential contrasts between the strain localization zones and their host rocks will also drive reaction softening processes in host rocks with fluids migration (e.g., Goncalves et al., 2016), leading to widening of the SLZs. Some other scholars, however, suggested that the widths of small-scale shear bands do not change after formation, and their widths are determined by the alteration haloes surrounding fracture precursors (e.g., Pennacchioni & Mancktelow, 2007). Variations of the widths of SLZs may be closely related to changes in deformation environments during the long-term geological history. Some of the SLZs may also be thinned during exhumation of the host rocks (e.g., Behr & Platt, 2011).

Another striking feature of the mid-crustal deformation is the coexistence of ductile and brittle deformation. Last decade, with the development of high-sensitivity seismographs and the improvement of geodetic networks, it has been found that aseismic slips, earthquakes, low-frequency earthquakes, tremors, and slow-slip events coexist in the subduction zones. They accommodate fault displacement and release energy together (e.g., Cristiano et al., 2011), indicating that faults have very complex rheological behaviors. It is also shown from seismic observations and field geological surveys that many earthquakes, especially large earthquakes occurred at the brittle-ductile transition zone (BDT) (e.g., Andersen et al., 2008; Austrheim & Andersen, 2004; Behr & Platt, 2011; Ferrand et al., 2017; Lin et al., 2003; Melosh et al, 2018; Rowe & Griffith, 2015; Shaw & Allen, 2007; Steward & Miranda, 2017; Swanson, 2006b Price et al., 2012; White, 2012). Although it is generally accepted that frictional slip or stick-slip processes are responsible for the seismic processes in the brittle domain or at the top of BDT, mechanisms of earthquake faulting at the base of BDT are still highly debated. The following two models have been proposed to explain seismic activities at the base of BDT: 1) top-down model: coseismic fractures originated from brittle domain propagate downward into BDT, causing sudden stress release and increase in strain rates, which result in ductile to brittle transition deformation with development of pseudotachylites and cataclasites (e.g., Allen, 2005; Allen & Shwa, 2011; Lin et al., 2003; Lin et al., 2005; Moecher & Steltenpohl, 2009; Price et al.,

2012; Shaw & Allen, 2007; Sibson, 1980; Trepmann & Stöckhert, 2013); 2) ductile instability model: fracture nucleation and velocity weakening processes develop during mylonitization at the base of BDT, accompanying the development of pseudotachylites (e.g., Hobbs et al., 1986; Hobbs & Ord, 1988; Meloshet al., 2018; Stewart & Miranda, 2017; White, 1996; White, 2012).

As indicators of seismic faulting, pseudotachylites, and their tempo-spatial and genetic relationship with deformation of their host rocks may provide key information on the paleo-earthquake processes. In this study, we investigate the deformation characteristics of recrystallized pseudotachylites that derived from biotite-plagioclase gneisses subjected to mid-crustal shearing at the base of BDT along the Jinzhou detachment fault zone of the Liaonan metamorphic core complex, North China craton. Influence of existence of rheological weak-phase, such as biotite, is addressed in discussing the formation and evolution of strain localization zones, and possible triggering mechanisms of paleo-earthquake faulting.

2 Geological setting

The late Mesozoic tectonics of the North China Craton, as exemplified by the Liaodong peninsula, is characterized by crustal extension and lithospheric thinning. A series of extensional structures are distributed in the Liaodong peninsula, e.g., the Liaonan metamorphic core complex (MCC), the Dayingzi detachment fault, the Tongyunpu and Benxi half garden basins. Their widespread occurrence is an indication of tectonic-thermal perturbation of crustal rocks in the peninsula in early Cretaceous (e.g., Liu et al., 2005, 2011, 2013).

The Liaonan MCC is constituted of three parts (Fig. 1), i.e., Jinzhou detachment fault (JDF), Archean metamorphic rocks (trondhjemite, tonalite, and granodiorite, zircon U-Pb LA-ICPMS ages are 2501±17Ma and 2436±17Ma (e.g., Lu et al., 2004)) and Early Cretaceous syn-kinematic intrusions in the lower plate, and weakly deformed Neoproterozoic-lower Paleozoic sedimentary rocks and a Cretaceous volcano-sedimentary basin in the upper plate. Thermal-chronological studies revealed the initial shearing along JDF and exhumation of Liaonan MCC before ca. 134 Ma (e.g., Liu et al., 2005, 2011, 2013). There were two stages of exhumation of the lower plate of the MCC, an early slow exhumation accompanied by giant magmatic events from before 130 Ma to 120 Ma and a rapid exhumation from 120 Ma to 113 Ma. The final scenario of the exhumation of the MCC occurred at ca. 107 Ma (e.g., Ji et al., 2015; Liu et al., 2005, 2011, 2013; Yang et al., 2007).

The Jinzhou master detachment fault (200 km in length) has an arcuate map trace, striking NNE and dipping to WNW in the western part (Jinzhou detachment fault), and striking ENE and dipping to the south in the southern segment (Dongjiagou ductile shear zone). Dip angles of the fault and shear zone vary from 20° to 40°. Both structures have stretching lineations plunging 110-130° or 290-310° (Fig. 1). Shear sense indicators from sheared rocks, e.g., asymmetrical fold, mica fish, S-C or S-C’ fabrics and σ or δ porphyroclasts indicate top-to-the NWW shearing.

The Jinzhou master detachment fault is located between the weakly deformed Neoproterozoic-lower Paleozoic sedimentary rocks and strongly deformed Archaean gneisses. A sequence of fault-related rocks of more than 5km in thickness were formed beneath the detachment fault surface, including deformed migmatites, mylonitic gneisses, banded or laminated mylonites, augen mylonites, brecciated mylonites, chloritic microbreccias,

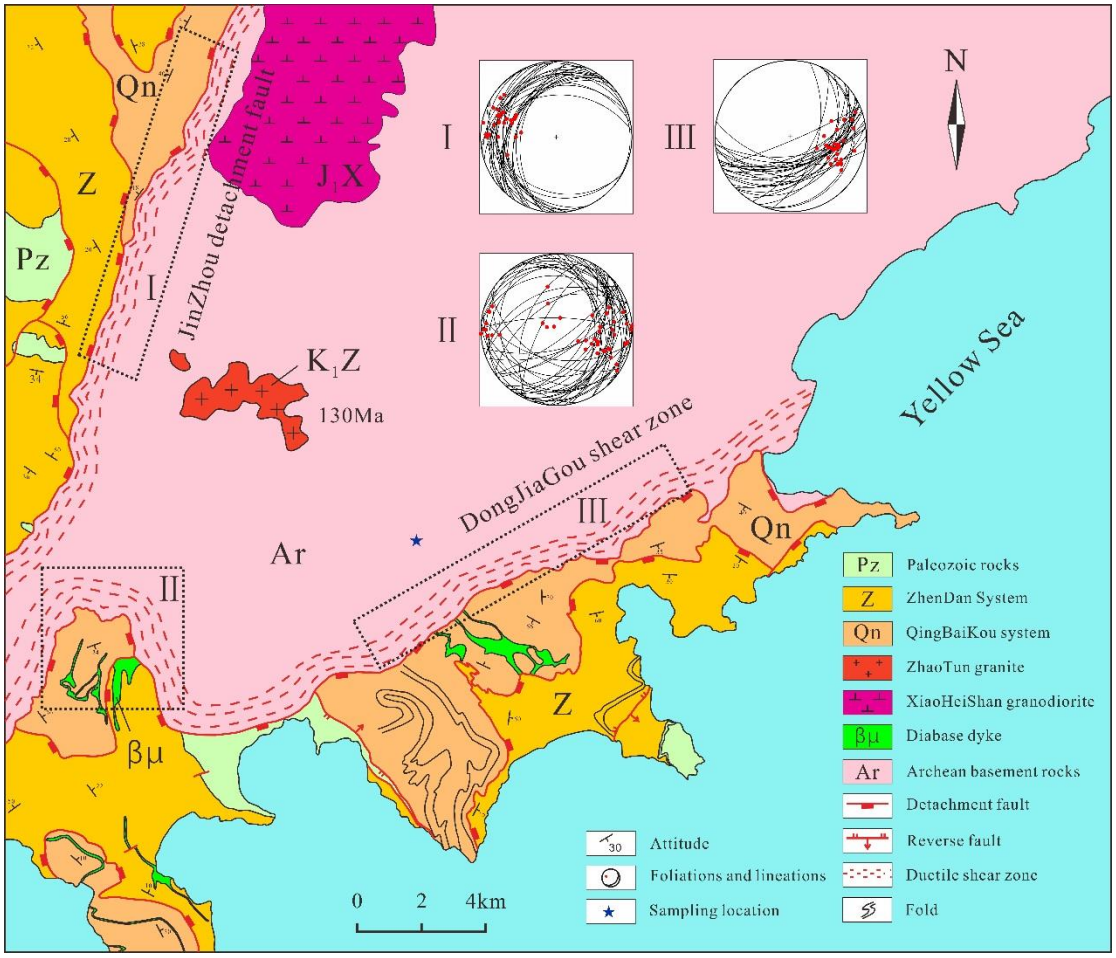

Figure 1. Geological map of Liaonan metamorphic core complex and sampling location. I-III are the equal area stereographic projection of foliations and lineations in three different areas (dotted boxes).

ultracataclasites, and fault gouges. They record deformation characteristics from upper amphibolite facies to lower greenschist facies. Microstructural and quartz C-axis crystallographic preferred orientation (CPO) fabric evidences from different rocks support progressive shearing from high (e.g., grain boundary migration of quartz, myrmekite) to medium (e.g., bulging recrystallization of quartz, undulose extinction) temperatures during detachment faulting. They are indications of strain localization during progressive exhumation of the lower plate. Besides, evidences for transient deformation, e.g., pseudotachylites, are also widespread along ductile shear zone. Both the sequential development of tectonites and evidences for transient deformation may provide important insight into processes of brittle-ductile transition and strain localization at the middle crust.

3 Techniques

Detailed field geological survey was conducted to investigate the mesoscopic deformation characteristics of the sheared rocks and their relationships. Oriented samples of fault rocks with different deformation characteristics were taken. Samples were cut parallel to stretching lineations and perpendicular to foliations. The samples without obvious lineations are cut according to the stretching lineation and foliation of the host rocks or in contiguous areas.

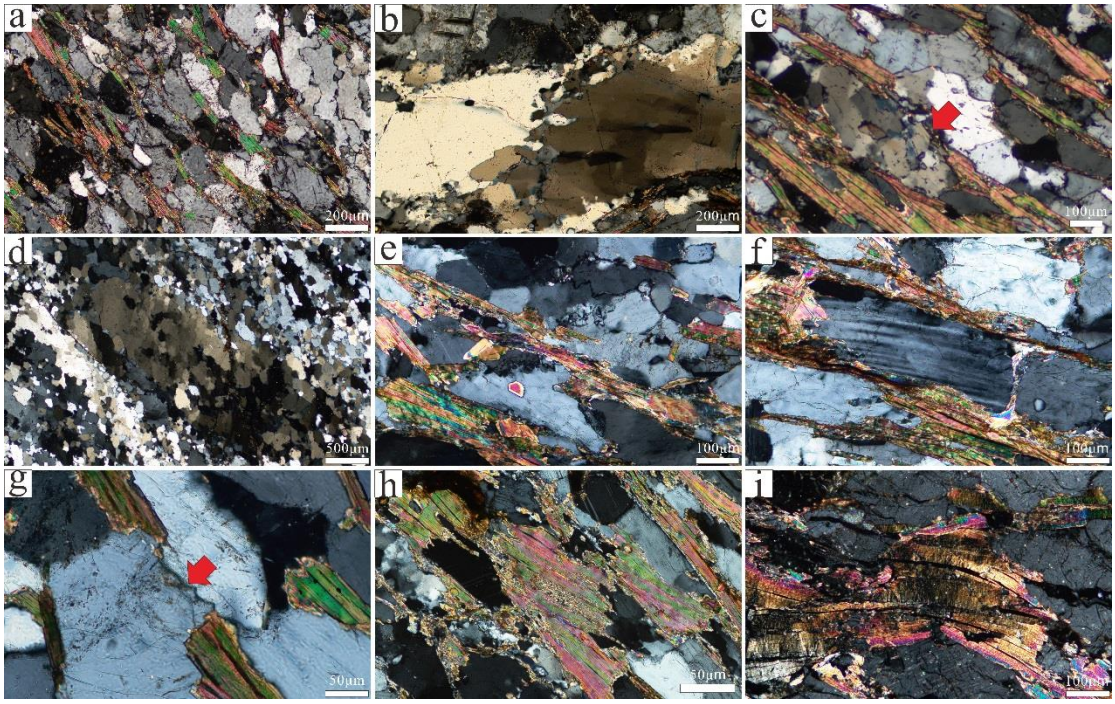

Figure 2. Microstructures of mylonitic gneisses. (a) Overview of mylonitic gneisses, feldspar grains constitute the load-bearing framework, isolated or weakly interconnected biotite form foliations. (b) Typical quartz grains in mylonitic gneisses. The chessboard subgrains and lobate grain boundaries were developed, indicating high-temperature deformation. (c) The quartz grain at the tips of biotite grain shows strongly undulose extinction and microcrack (red arrow), indicating stress concentration. (d) Quartz ribbon developed in mylonitic gneisses, subgrains are well developed in quartz porphyroclast, lobate grain boundaries between recrystallized grains imply the operation of grain boundary migration. (e) Myrmekite at the edges of K-feldspar grains indicates high-temperature deformation. (f) Interconnected biotite grains and mechanical twins in feldspar grainsduo to ductile deformation. (g) Microcrack (red arrow) at the tips of biotite grains indicate stress concentration. (h) Fine-grained aggregates are developed in the interiors of biotite grains. (i) kink bands and undulose extinction in the biotite grains.

Thin sections were polished using Buehler mastermet colloidal silica and Buehler grinder-polisher to remove the damaged lattice during mechanical polishing. The thin sections were gold-coated for scanning electron microscopy (SEM) and electron backscatter diffraction (EBSD) observations and measurements. SEM and EBSD measurements are mainly performed on Hitachi S-3400NII SEM fitted with Nordlys Model NL-II detector at the State Key Laboratory of Geological Processes and Mineral Resources of China University of Geosciences (Beijing) and Zeiss-sigma SEM equipped with Oxford-Nordlys Nano detector at State Key Laboratory of Earthquake Dynamics of Institution of Geology, China Earthquake Administration. The acquired EBSD data were processed using HKL Channel 5 software package.

4 Results

There are three types of deformed gneissic rocks with obviously different characteristics, i.e., widespread low-strain zones (LSZs) (Figs. 2 and 7c, d), narrow SLZs (Fig. 4), and pseudotachylite veins in the SLZs (Fig. 6). SLZs and pseudotachylites veins are concordant with

the foliations in mylonitic gneisses. The detail characteristics of LSZs, SLZs, and pseudotachylite veins and their relationships are described in following sections.

4.1 Minerals deformation in the low-strain zone

Mylonitic gneisses, protoliths of biotite-plagioclase gneisses are dominant rocks in the LSZs. They are composed of plagioclase (45±5 vol%), quartz (25 vol%), biotite (15 vol%) and K-feldspar (10 vol%), and minor epidote, muscovite and hematite. Feldspar grains constitute the load-bearing framework in the sheared gneisses (Figs. 2a, 7c). The separate biotite grains constitute the foliation of gneisses. Meanwhile, some biotite grains are interconnected and form the biotite-rich layers embedded in the framework (Figs. 2a, 7c).

4.1.1 Plagioclase

Plagioclase grains have irregular morphology and grain boundaries (Fig. 2a). They have obvious shape preferred orientation (SPO) that is nearly parallel to the foliations, and have an average aspect ratio up to 2 (Fig. 7c). Undulose extinction and curved mechanical twins are observed in the plagioclase grains (Figs. 2e, f). Some plagioclase grains show intragranular fractures and fragmentation, particularly when the grains are located at the tips of biotite grains. Intragranular and intergranular microcracks are often filled with micas and fine-grained feldspar grains (Figs. 7e-h).

4.1.2 Quartz

Quartz grains are in two forms in the mylonitic gneisses, i.e., individual grains (Figs. 2a-c) and polycrystal quartz ribbons (Fig. 2d). Individual grains generally have irregular shapes and serrated grain boundaries. The average aspect ratios are ca. 2, with long axes nearly parallel to the foliations (Figs. 2a-c). Undulose extinction, lobate grain boundaries, and chessboard sub-grains are well preserved in these grains. Some individual quartz grains contain fluid inclusions planes (FIP) that always cut across the lobate grain boundaries. Quartz grains at the tips of biotite grains show irregular grain boundaries, strong undulose extinction and sometimes intragranular microcracks (Figs. 2b, c). The crystallographic preferred orientations (CPO) patterns of individual quartz grains show an asymmetric crossed-girdle, similar to type I crossed-girdle of e.g., Lister and Williams (1979), and are indicative of clockwise shear sense (Fig. 3a). The quartz grains in quartz ribbons are almost completely recrystallized. Subgrains are well developed in quartz porphyroclasts. The grain sizes of subgrains are smaller than those of recrystallized grains. The latter show minor intragranular deformation and have lobate grain boundaries due to grain boundary migration (GBM) (Fig. 2d). The C-axis fabrics of the recrystallized quartz grain feature monoclinic symmetric patterns and are also indicative of clockwise shear sense. The two main maxima between the Y-and Z-axes, are attributed to rhomb <a> slip, while the Z-axis maxima are resulted from basal <a> slip. Both of them imply noncoaxial shearing at medium to low temperatures (Fig. 3b).

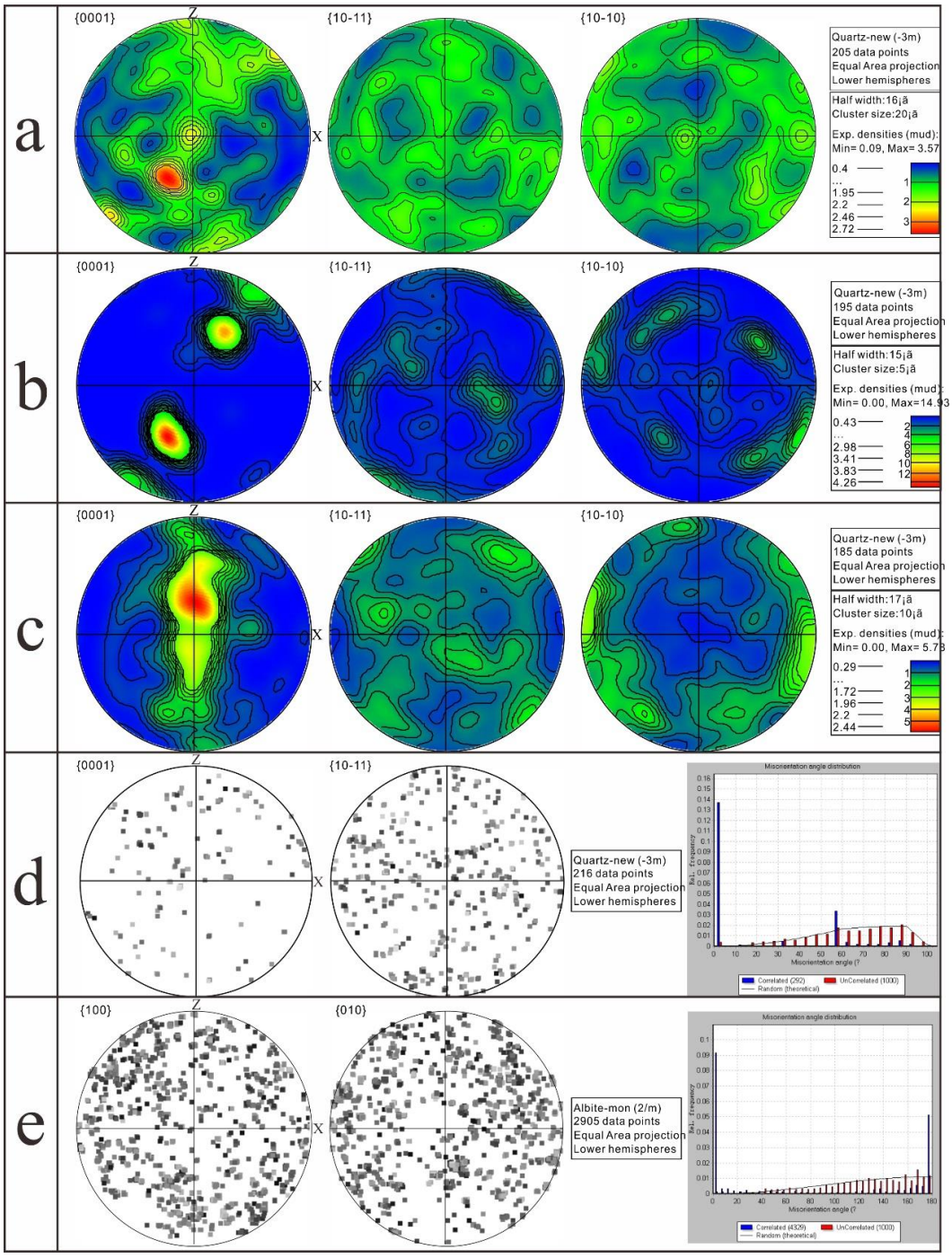

Figure 3. Pole figures of crystallographic-preferred orientation (CPO) of quartz and plagioclase grains in the low-strain zones and high-strain zones. (a) The CPO of individual quartz grains in mylonitic gneisses show type I crossed-girdle, indicating clockwisedextral shear sense. (b) The CPO of quartz ribbon in mylonitic gneisses show monoclinic symmetric patterns. The two main maxima between the Y-and Z-axis, are attributed to rhomb <a> slip. The Z-axis maxima were formed by basal <a> slip. (c) The CPO of quartz lenses in high-starin zone, C-axis distribute along the Y-Z plane. (d) The CPO and misorientation angle distribution curve (MAD) of quartz grains in SLZs, the CPO show random distribution, the curve is consistent with theoretical ransom curve, both of them indicate the operation of grain boundary sliding (GBS). (e) The CPO and MAD of plagioclase grains in SLZs, both of them imply the operation of GBS

212 4.1.3 K-feldspar

213 Backscatter electron (BSE) images show that K-feldspar grains have elliptical shapes,
214 obvious SPO, and irregular grain boundaries. Fine plagioclase and quartz grains of less than 5μm
215 are generally observed along the boundaries of K-feldspar grains. The plagioclase grains
216 generally have angular shapes, and their long axes are nearly perpendicular to the surface of the
217 host K-feldspar grains (Fig. 4a). Quartz grains are filled between plagioclase grains, such as
218 triple junction or mircopores (Figs. 4a, d). The microcracks inside the K-feldspar grains are
219 common, but these microcracks do not cut across the fine-grained plagioclase and quartz grains
220 (Fig. 4a). On the contrary, fine-grained plagioclase grains often develop along the intragranular
221 microcracks (Figs. 4a, d, e). Angular fine-grained K-feldspar grains are also observed inside
222 coarse K-feldspar grains (Figs. 4a, d). The results of EBSD mapping of host K-feldspar grain and
223 the fine-grained plagioclase and quartz aggregates (step size of 0.25μm) show a low indexing
224 rate in the fine-grained area and high indexing rate (>90%) in host K-feldspar grain, this result
225 can reflect the internal structure of K-feldspar grains. Low-angle grain boundaries (2-10º) inside
226 the K-feldspar grains are not observed. Some straight low-angle grain boundaries are, however,
227 intragranular fractures (Fig. 4c); Angles between host K-feldspar grains and fine-grained
228 plagioclase grains are generally less than 10º (Fig. 4b). Meanwhile, host K-feldspar grains and
229 fine-grained plagioclase grains have similar CPO's (Figs. 4h, f), while the C-axis fabrics of
230 quartz grains show random distribution (Fig. 4g). Besides, K-feldspar grains are often replaced
231 by plagioclase grains along their margins (Fig. 4e).

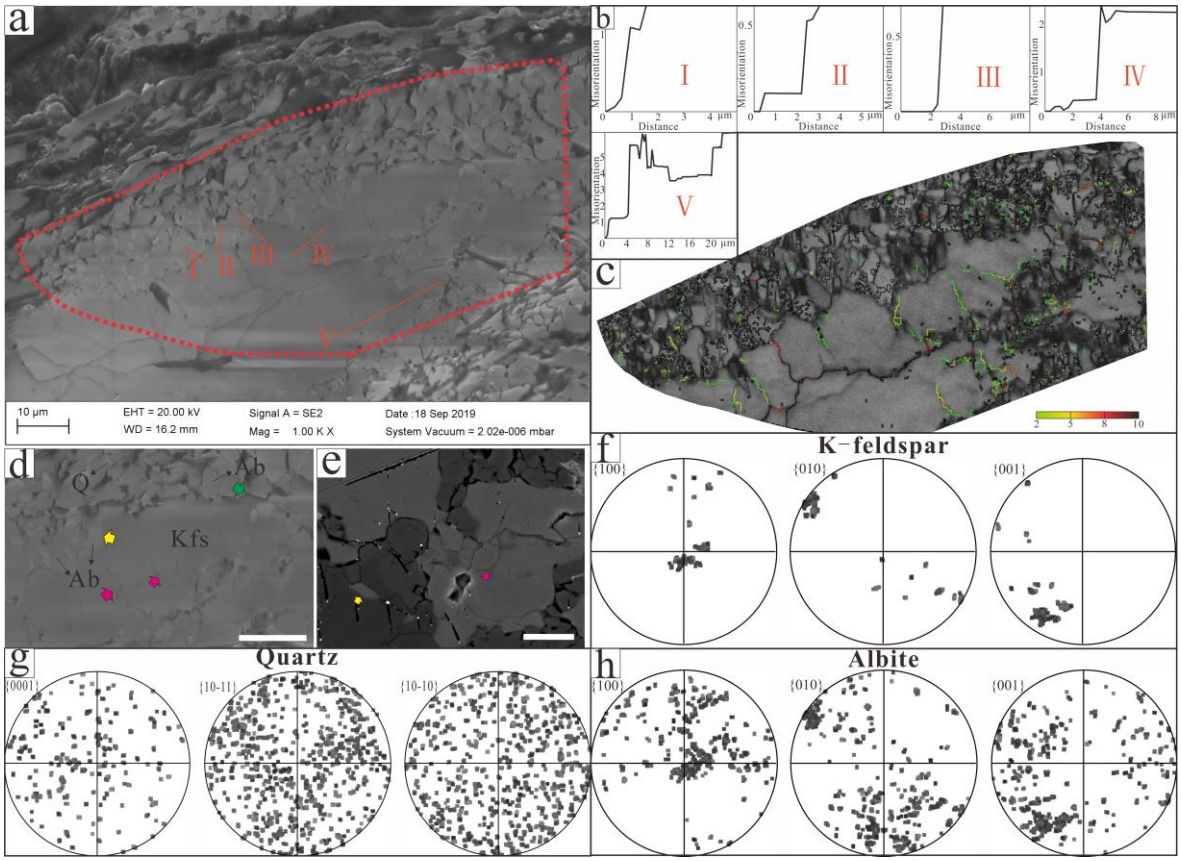

Figure 4. The microstructure of K-feldspar porphyroclast and the mixture of fine-grained plagioclase and quartz aggregates. (a) The SEM image of K-feldspar porphyroclast and the mixture of feldspar and quartz aggregates surrounding it. I-V are locations of the misorienattion profiles related to first point, dotted box is

the location of EBSD measurement. (b) Misorientation profiles in different sections.I-III indicate very low misorientation angles between plagioclase grains and the host K-feldspar porphyroclasts, IV indicates very low misorientation angle between angular fine-grained K-feldspar grains inside the porphyroclast. V indicates low misorientation between host grain and sungrains surrounded by low angle grain boundaries. (d)-(e) Green arrows indicate angular shapes of fine-grained plagioclase grains, yellow arrows indicate that K-feldspar grains are replaced by plagioclase, pink arrows indicate the microcracks inside the K-feldspar porphyroclasts. (f) The CPO of K-feldspar porphyroclast. (g) The CPO of fine-grained quartz grains between fine-grained plagioclase grains, the pole figure show nearly random dietribution. (h) The CPO of plagioclase is similar to the CPO of host K-feldspar porphuroclast.

232 #### 4.1.4 Biotite

233 Biotite grains are nearly homogeneously distributed along foliations in the mylonitic
234 gneisses. Some of the biotite grains are weakly interconnected (Figs. 2a, 7c, d). The grains have
235 aspects ratio up to 4-5. Kink bands and undulose extinction are well-developed in the biotite
236 grains (Figs. 2h-i). Some fine-grained aggregates are found along the grain boundaries and
237 interiors of biotite grains (Fig. 2h). BSE imaging reveals that these aggregates are mixtures of
238 fine-grained feldspar and biotite grains. Some micro-shear zones are observed within the biotite
239 grains. Some of the biotite grains are replaced by muscovite along these micro-shear zones (Figs.
240 5b, c).

241 ### 4.2 Strain localization zones

242 The SLZs are narrow, mica-rich zones with variable widths (less than 5mm). Some of
243 them were overprinted by pseudotachylite veins. Microstructural analysis shows that the initial
244 SLZs only consist of biotite grains and microcracks at the tips of biotite (Figs. 7e, f), while
245 mature SLZs are composed of biotite, muscovite, and fine-grained plagioclase and quartz grains
246 (Figs. 5b, c). Some elliptical K-feldspar porphyroclasts surrounded by mixtures of fine-grained
247 plagioclase, quartz and biotite grains also appear in SLZs (Fig. 5b). There are three distinct
248 mineral combinations in the mature SLZs. Type I consist of biotite and muscovite grains with
249 subhedral shapes. Some micro-shear zones composed of muscovite grains appear in biotite
250 grains (Figs. 5b, c). Type II: Angular plagioclase grains and disordered mica grains are
251 widespread, which is similar to fault gouge. They always occur along the boundaries between the
252 high-strain and low-strain zones (Figs. 5b-d). Type III: Aggregates of small plagioclase grains
253 have grain-size of ca. 10μm and aspect ratios of 1-2, respectively. Their long axes have low
254 angles (less than 20º) foliations. It is noteworthy that there are a lot of mircopores along the grain
255 boundaries. Some of the mircopores are filled with quartz and biotite grains (Fig. 5c). The CPO's
256 of plagioclase and quartz grains in SLZs show random distribution pattern. Their misorientation
257 angle distribution curves are consistent with theoretical random curve of uncorrelated grains
258 (Figs. 3d-e).

259

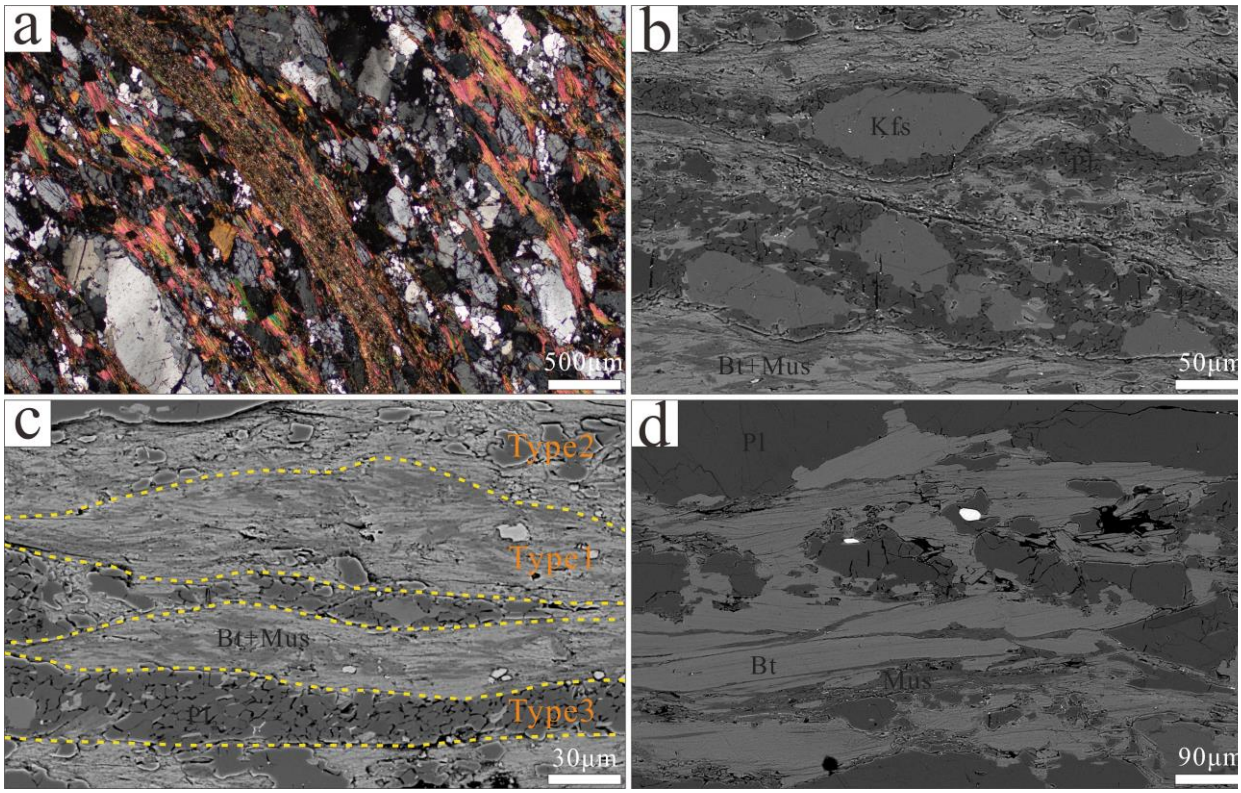

Figure 5. Microstructures of high-strain zones. (a) Overview of SLZs. (b)-(d) The BSE images of SLZs. (b) K-feldspar porphyroclasts are surrounded by the matrix of fine-grained plagioclase, quartz and biotite grains. (c) Three distinct type of mineral combination, type I: the mixsture of biotite and muscovite grains with subhedral shape, type II: the mixture of angular plagioclase grains and disordered biotite grains, which is similar to fault gouge, type III: the fine-grained plagioclase aggregates. (d) The micro-shear zones developed in biotite grains.

4.3 Pseudotachylite

Pseodotachylite veins are nearly parallel to the foliations in the gneisses. They are always located in SLZs. They have clear and irregular boundaries with host rocks. Their widths vary between 3 and 10 mm (Fig. 6a). Microscopic observations show that the pseodotachylites are completely recrystallized. The veins are presently mainly composed of mixtures of plagioclase, biotite and quartz grains with grain sizes of ca. 3μm (Fig. 6d). There are some crystal fragments, e.g., plagioclase, quartz, and garnet, which have elliptical or angular shapes, diffusive boundaries, within the fine-grained matrix. The fragments do not possess tails as those in the mylonites or ultramylonites (Figs. 6b, c). Mechanical twins and undulose extinction are observed within the plagioclase and quartz fragments (Figs. 6b-c). It is shown that the pseudotachylites were subjected to ductile deformation after their formation that the recrystallized biotite grains were aligned to form foliations. Nanograins appear in some mircopores of recrystallized pseudotachylites. They have spherical shapes with grain sizes of less than 100 nm (Fig. 6e). EDS components analysis demonstrate that these nanograins have different compositions, but similar to quartz. Some residual amorphous materials are observed in pressure shadows of the plagioclase fragments. EDS components analysis shows that their compositions are complex and vary greatly, but all contain high contents of Mg, Fe, and Ti.

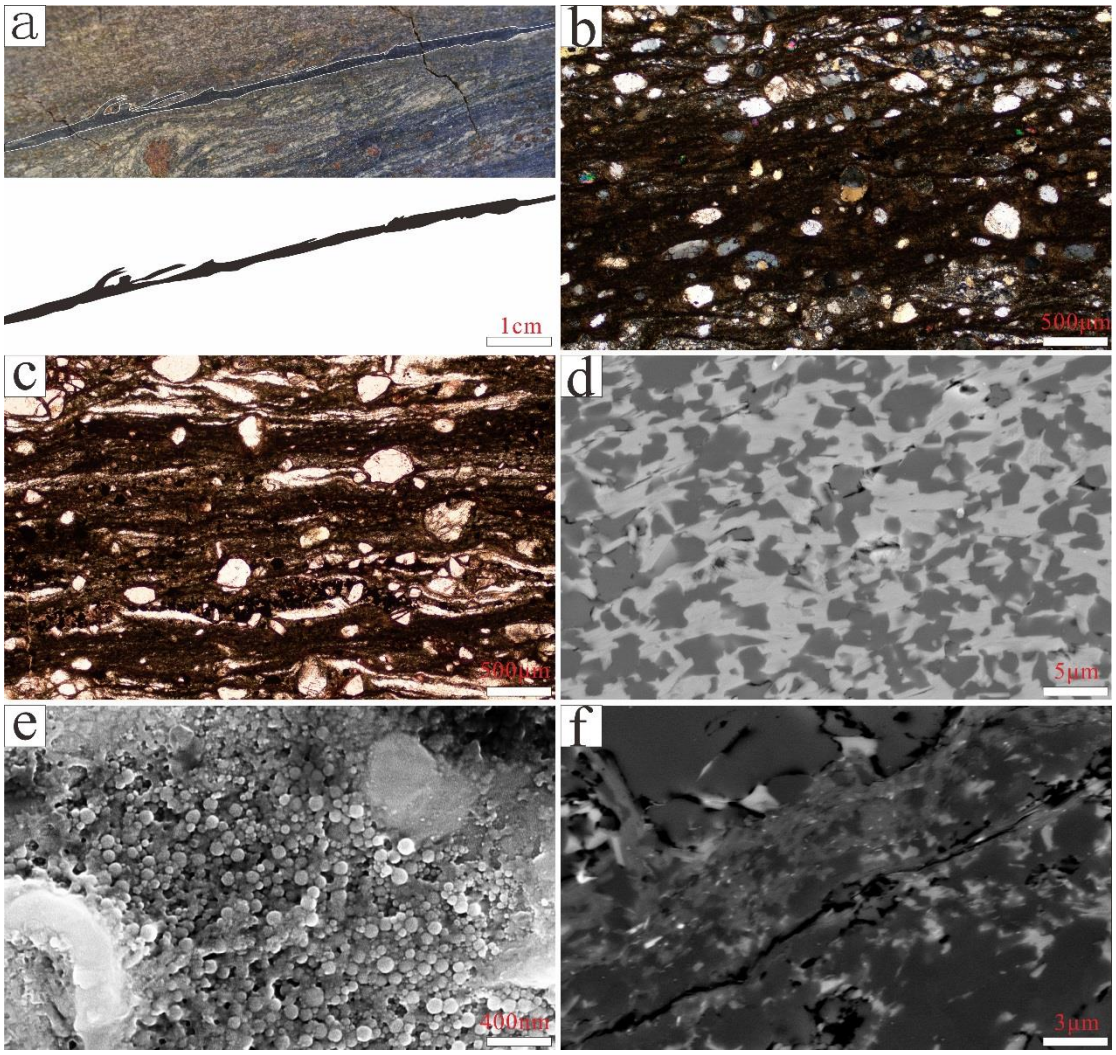

Figure 6. The characteristics of pseudotachylite. (a) Outcrop-scale features of pseudotachylite vein, pseudatachylite vein has sharp and irregular boundaries, where injection veins also appear. (b)-(c) are micrographs of pseudotachylite under optical microscope, quartz lenses show SGR; the clasts show diffuse boundaries, angular or rounded shapes and no trail. (d) The BSE image of recrystallized pseudotachylite which consists of ultra-fine-grained biotite and plagioclase grains. (e) Nanograins formed in the mircopores, they have rounded shapes, residual feldspar grains have embayed shaped. (f) Amorphous materials preserved in strain shadow.

5 Discssion

5.1 Deformation mechanisms of quartz, feldspar grains

The above microstructural observations reveal that various mechanisms of deformation contributed to the deformation of quartz grains in the gneissic rocks. Quartz grains in the low-strain zones show microstructures and fabrics, e.g., undulose extinction, sub-grains, and strong CPO, compatible with dislocation creep (e.g., Hirth & Tullis, 1992; Richard, 2014; Stipp et al., 2002). The appearance of FIPs in quartz grains suggests that they have experienced brittle fracturing and post-fracturing healing processes. Some quartz grains at the tips of biotite grains exhibit semi-brittle flow (Fig. 2c), such as fractures or stress corrosion cracking (e.g., Barnett

and Kerrich, 1980; Kerrich et al., 1981). The microstructural differences between quartz grains at different locations relative to biotite grains reflects differential stress concentration, higher at the tips but lower at the other parts of biotite grains (e.g., Holyoke & Tullis, 2006). The random CPO's of quartz grains, as well as their misorientation angle distribution curve are consistent with the theoretical random curve of uncorrelated grains, indicating the operation of GBS in the high-strain zones (e.g., Kilian et al., 2011; Lopez-Sanchez & Llana-Fúnez, 2018).

The plagioclase grains mainly underwent semi-brittle flow in low-strain zones. The grain-scale fractures are more common in plagioclase grains located at the tips of biotite grains than other plagioclase grains. The nucleations of the intragranular microcracks at these locations indicate that the stresses at the tips of biotite grains are higher than those in other locations during the deformation. Stress concentrations are suggested to result from the high phase strength contrasts (PSC) between the feldspar grains and the biotite grains (e.g., Holyoke & Tullis, 2006). The appearance of undulose extinction and mechanical twins in plagioclase grains suggests that ductile deformation of the grains also occurs contemporaneously (e.g., Tullis & Yund, 1985; Kruse et al., 2001). It is therefore suggested that the deformation of the feldspar and thus the rocks occurred at the brittle-ductile transition. The random CPO and nearly random misorientation angle distribution curve of feldspar grains in the high-strain zones imply the operation of GBS. (e.g., Fukuda & Okudaira, 2013). The presence of mircopores between the grains indicates that dissolution-precipitation or diffusion creep is insufficient to accommodate the mircopores created during GBS. The appearrance of mircopores is a sign of the transition from steady-state slip (velocity strengthening) to unstable slip (velocity weakening), and has the potential to trigger earthquakes at depths (e.g., Verberne et al., 2017). Many experimental studies addressed that biotite grains are very easy to be deformed by basal plane slip, and hard to be broken (e.g., Kronenberg, 1990). However, the appearance of type II mineral combinations and micro-shear zones in biotite grains from SLZs imply the dominance of frictional slip along the SLZs.

K-feldspar grains are often surrounded by mixture of fine-grained plagioclase and quartz grains (Figs. 5b, 4a). These plagioclase grains have angular shapes and preferentially develop along the intragranular microcracks, indicating that these grains are associated with fragmentation. The results of the EBSD mapping of K-feldspar porphyroclasts and fine-grained plagioclase and quartz grains in the matrix showed that: 1) There are few low-angle grain boundaries within the porphyroclasts, indicating that dislocation organization is not the well-developed in the porphyroclasts. Sparse occurrence of low-angle grain boundaries is related to intragranular microcracks (Fig. 4c), which is similar to the experimental results for plagioclase and quartz aggregates in the brittle-ductile transition field (e.g., Hirth and Tullis. 1994; Mcalren and Pryer, 2001). On one hand, microcracks may be nucleated due to dislocation pileups in response to stress concentration. On the other hand, microcracks would also promote dislocations slip at their tips (e.g., Hirth & Tullis. 1994; Mcalren & Pryer, 2001). 2) The CPO's of the fine-grained plagioclase grains and the host K-feldspar porphyroclasts are similar to each other (Figs. 4f, h), and the misorientation angles between them are generally smaller than 10º. These evidences do not support a mechanism of typical dislocation creep, because new grains formed by BLG or SGR mechanisms tend to have an equiaxed morphology and misorientation angles higher than 10º with the host porphyroclast, and related dislocation organization processes are common within their host porphyroclasts (e.g., Hirth & Tullis, 1992; Richard, 2014; Stipp et al., 2002). Hence, we suggest that these fine-grained plagioclase grains are not formed by the dislocation organization process. Furthermore, some angular fine-grained K-feldspar grains with

similar grainsizes and shapes with fine-grained plagioclase grains also appear along the margins of the K-feldspar porphyroclasts (Fig. 4d). Some angular fine-grained K-feldspar grains and K-feldspar porphyroclasts are replaced by plagioclase grains along their edges (Figs. 4d-e). From the above evidences, we therefore suggest that the fine-grained plagioclase and quartz matrix grains are formed by the following processes: 1) At first, fine-grained K-feldspar aggregates formed along the margins of K-feldspar porphyroclasts due to fragmentation. Microcracks provide channels for fluid infiltration. Fine-grained K-feldspar grains have higher surface area, that they are more easily replaced than their host porphyroclasts. Fine-grained K-feldspar grains are therefore transformed into an assemblage of plagioclase and quartz grains, similar to the formation of myrmekites in k-feldspars (e.g., Simpson & Wintsch, 1989; Menegon et al., 2006).A non-negligible fact is that a lot of fine-grained plagioclase grains surrounding the K-feldspar porphyroclasts possess equiaxed grain shapes and smooth grain boundaries (Figs. 4c, 5b). Therefore, fragmentation may not be the only mechanism of grain size reduction.

5.2 Mechanisms of fluid migration

Fluids have important influences on deformation of rocks at middle crust. They may promote dislocation creep, lead to metamorphic reactions and enhance dissolution-precipitation, but also reduce effective confining pressures (e.g., Chernak et al., 2009; Liu et al., 2002; Mancktelow & Pennacchioni, 2004; Tullis et al., 1996; Yund & Snow, 1989; Wibberley, 1999; Wintsch et al., 1995). Recent studies suggest that pore fluids migrations have been invoked to explain tremor and stress transfer across the BDT (e.g., Melosh et al., 2016; Steward & Miranda, 2017). Several models have been proposed to interpret the migration of fluids during deformation, e.g., seismic pump models (e.g., Sibson et al., 1975; Weatherley & Henley, 2013), rotation of breccia (e.g., Melosh et al., 2016) and creep cavitation (e.g., Fusseis et al., 2009; Menegon et al., 2015) etc. The former two mainly appear in the brittle domains, while the latter operates in ductile domain. Creep cavitation is a self-sustained process during GBS, where a permeable porosity is dynamically created by granular flow (e.g., Fusseis et al., 2009). However, GBS does not always occur in all mylonites. It is shown in the present study that microcracks were developed at the tips of the biotite grains accompanying the fragmentation of feldspar grains during initial deformation. Fluids-involved processes occurred along the microcracks, e.g., precipitation of biotite grains, replacement of biotite and K-feldspar grains by muscovite and plagioclase grains. However, these processes were not observed at other positions of the grains (Figs. 5b, 7b). It is hence suggested that the development of microcracks in the early stage of deformation processes controls the migration of fluids within the shear zones. The development of the microcracks increases the porosity and permeability, but also creates local low-pressure domains in the rocks. The pressure contrasts drive further migration of fluids in the rocks. As grainsizes are reduced, new microcracks no longer develop. However, intensive fluid/rock interactions are still active along the SLZs by, e.g., precipitation of biotite and quartz grains between fine-grained plagioclase grains (Fig. 5c). These evidences suggest that creep cavitation may be the dominant mechanism of fluid migration in the rocks at this stage after the occurrence of GBS (e.g., Fusseis et al., 2009).

5.3 Nucleation and widening of strain localization zone

How SLZs are formed in homogeneous rocks, e.g., granites, or heterogeneous rocks, e.g., gneisses, is an important topic in understanding the rheology of middle-lower crust and earthquake faulting. Comprehensive studies on the topic may help us to understand the processes

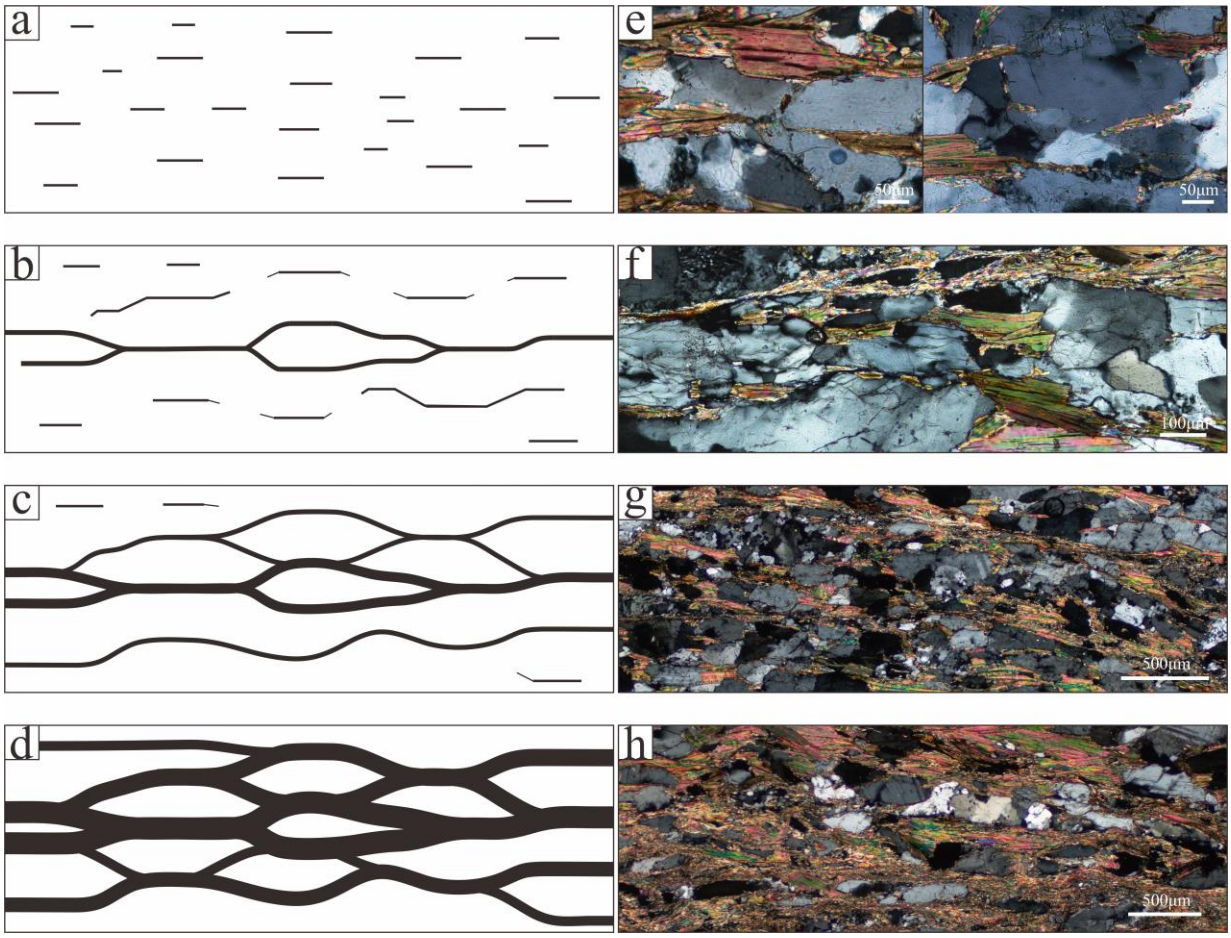

Figure 7. Schematic illustration of the evolution of SLZs (Inspired by Fossen and Cavalcante (2017)). (a) Undeformed gneisses. (b) Initial SLZs and microcracks at the tips of biotite grains. (c) and (d) Initial SLZs merge with each other, causing the widening of SLZs. (e) Microcracks at the tips of biotite. (f) Interconnection of microcracks. (g) and (h) the widening of SLZs.

of formation of crustal or lithospheric scale fault zones (e.g., Gueydan & Frédéric, 2003). Several mechanisms have been proposed to explain the formation and evolution of SLZs. The transition from the LBF to IWP is considered to be the most important mechanism for the strain localization in polyphase rocks (e.g., Fukuda & Okudaira, 2013; Gueydan & Frédéric, 2003; Mansard et al., 2018; Oliot et al., 2014; Wibberley, 1999; Wintsch et al., 1995; Wintsch & Yeh, 2013). However, how this transition is accomplished in the polyphase rocks at the middle crust is still under debate. The mechanisms of deformation of different mineral phases and governing mineral phases in the transition are the two fundamental questions to be answered.

Gneisses are the dominant rock types in the middle and lower crust. Therefore, the studies on mechanisms of strain localization in gneisses are of great significance for us to understand the rheology and the faulting mechanisms in the middle and lower crust. Our results show that partly or completely interconnected biotite-enriched zones with variable width are characteristic of LBF in low-strain zones (Fig. 7). Increasing degrees of interconnection and width of the IWPs are consistent with the transition from protomylonites to mylonites and ultramylonites. We therefore argue that IWPs with different degree of interconnection and width are snapshots of different stages of the formation and evolution of SLZs. Stage 1: Intragranular

and intergranular microcracks were formed at the tips of biotite grains due to stress concentrations (Figs. 7b, e). Stage 2: The existing microcracks propagate and are interconnected (Figs. 7c, f). At this stage, the microcracks often cut through several biotite grains, and no significant displacement occurs along the interconnected microcracks Stage 3: As propagation and interconnection of the microcracks continue, displacements occur along the interconnected microcracks (Figs. 7b, c and g). The basal plane slip and GBS became active in biotite grains and in fine-grained plagioclase aggregates, respectively. They may lead to significant strain softening, where the initial strain localization zones were formed (Figs. 7c, h). The results of Holyoke and Tullis (2006) show that after the SLZs were formed, the strength would reduce by approximately a half, and the strain rate within the SLZs would be approximately 100 times than that of the host rocks. Stage 4: the broadening of initial SLZs (Figs. 7d, g and h). In stage 1, biotite grains govern the deformation of the rocks as pre-existing weak phase. Opening of microcracks at the tips of biotite grains indicates that differential stresses due to stress concentration have exceeded the confining pressures. If we assume a confining pressure of 476 MPa (deformation temperatures of ca. 450℃, rock density of 2.7×10^3 kg/m^3, geothermal gradient of 25℃/km), the numerical simulation results of Johnson et al. (2004) show that the stress concentration at the tips of biotite grains with similar aspect ratio of our biotite grains can reach up to 1.3 to 2 times confining pressure. Hence, the local stress can reach about 700 MPa, implying that the stress concentration far exceeds the differential stress calculated by recrystallized quartz size piezometer at the same depth (10-20 MPa from the result of Behr and Platt (2011)), and even the rheological strength at the BDT (200MPa). However, this value is lower than the value predicted by Holyoke & Tullis (2006). The reason is probably lower values of strain rates and confining pressures applied in the present study than those Holyoke and Tullis (2006) adopted. The stress concentration due to PSC between different phases during deformation and its leading role in promoting strain localization were not only found in the rocks containing biotite, but also were found in other polyphase rocks, such as granites, banded-iron formations (e.g., Dell'Angelo & Tullis, 1996; Goncalves et al., 2015).

The SLZs developed in the gneisses are originated from the interconnection of microcracks, so that their initial widths are very small. Variations in widths, however, imply that they undergo different degrees of widening after nucleation. Many experimental studies have shown that as strain increases, biotite layers would undergo strain hardening. However, their friction coefficients are still lower than that of quartz under the same conditions (e.g., Kronenberg et al., 1990; Shea & Kronenberg, 1992; Lu & He, 2014; Lu & He, 2018; Den Hartog et al., 2013). In addition, different mineral phases tend to be mixed with each other in our study as deformation continues. From the experimental results on quartz-biotite materials of Lu & He, (2018) show that the friction coefficients of interlayers of quartz-biotite-quartz grains are lower than those of quartz-biotite mixtures with the same mica contents. Therefore, the phase-mixing processes which occur both in experiments and in nature may also lead to strain hardening. However, S-C or S-C' fabrics representing strain hardening (e.g., Holyoke & Tullis, 2006) do not appear in the studied gneisses. Their absence implies that the strengths of SLZs are still lower than those of the host rocks, although strain-hardening processes occurred. It is worth noting that these strain hardening processes may result in higher strengths of mature SLZs than those of the initial SLZs. Thereby strain partitions into new initial SLZs are facilitated. Moreover, the lower strengths of the SLZs than those of their host rocks ensure their maintenance during progressive deformation. At the same time, the preservation of weakly interconnected microcracks on both sides of the SLZs may indicate that deformation processes of

the stages 1 to 3 further continue to occur in the host rocks after the formation of the SLZs. Besides, the newly formed initial SLZs continuously merged with the mature SLZs (Figs. 7c-d), which contribute to dramatic widening of the SLZs.

5.4 Ductile instability and coeval development of mylonites and pseudotachylites

Pseudotachylites which have undergone retrograde metamorphism and deformation in ductile shear zones, are generally difficult to be distinguished from ultramylonites (e.g., Kirkpatrick & Rowe, 2013; Lin et al., 2003; Lin et al., 2005; Price et al., 2012; Rowe & Griffith, 2005; White, 1996; White, 2012). The OM and SEM observations show that the black dense pseudotachylite veins in the present study have been completely recrystallized (Fig. 6). However, they are assured to be pseudotachylites by the following evidences: 1) The veins have sharp boundaries with their host rocks (Fig. 6a). 2) Injection veins often occur, although they also have undergone intensive deformation during post-veining deformation (Fig. 6a). 3) The thicknesses of the veins vary significantly along their extension; 4) The presence of amorphous materials in the pressure shadows of porphyroclasts. Some of them have been devitrified or recrystallized, forming crystallites with grainsizes of ca. 100 nm (Fig. 6f). EDS analysis shows that these amorphous particles are enriched in Mg, Fe, Ti, being consistent with the results from Lin, (2008). 5) Recrystallized pseudotachylites have extremely fine grainsizes of ca. 3μm and have higher biotite content than their host rocks (Fig. 6d). 6) The clasts have diffusive boundaries, subrounded shapes and do not have tails that are often present in mylonitic rocks (Figs. 6b-c).

Seismic observations indicate that there are a large number of seismic activities at the middle crust (e.g., Lin et al., 2005; White, 2012), or even at the base of BDT, e.g., 2017 Mw 7.0 Jiuzhaigou earthquake at ca. 20km; 2001 Ms 8.1 Central Kunlun earthquake at ca. 17km (Lin et al., 2005). Previous studies have proposed the Top-down model and the ductile instability model to interpret why frictional slip occur and pseodotachylites are formed at the base of or ductile domain. There have been no generally acceptable interpretations for the latter model (e.g., Hobbs et al., 1986; Hobbs & Ord, 1988; Stewart and Miranda, 2017; White, 1996; White, 2012), although the former model is supported by a large number of seismic observations and geological evidences (e.g., Lin et al., 2005). The very extreme difficulty in exploring the mechanisms of earthquakes by studying pseudotachylites and their host rocks in natural ductile shear zones is that we do not know of the focus depth of paleo-earthquakes. Another serious problem is that some evidences are not preserved during progressive deformation of the rocks in the middle to lower crustal levels (e.g., Rowe & Griffith, 2015). Recrystallization and ductile deformation of pseudotachylite veins imply that the veins are not generated by frictional slip in the brittle domain. The coexistence of initial SLZs and ductile-deformed pseudotachylite veins along SLZs indicates that the ductilly deformed pseudotachylite veins are formed coevally with or are slightly earlier than the initial SLZs. Moreover, the compositions of the recrystallized pseudotachylite veins are similar to those of the ultramylonites in the SLZs (Figs. 5b, c; 6d), and the deformation characteristics of the clasts are also consistent with the host rocks (Figs. 2; 6b). These evidences suggest that the SLZs and pseudotachylite veins are formed at identical environments. Besides, the foliations in the pseudotachylite veins are nearly parallel to the foliations in the host rocks. It is therefore concluded that the pseudotachylite veins and the SLZs are spatially, temporally and genetically related to each other. The occurrence of pseudotachylite veins within the core of the SLZs, and the absence of cataclasis associated with the veins imply that the SLZs are the ductile precursors of the pseudotachylite veins (e.g., White, 2012). In other words, frictional slip that generated the pseudotachylite veins occurred along with the SLZs, i.e.,

the micro-shear zones in biotite grains, type 2 mineral combination zones in the SLZs, and the FIPs developed in quartz grains. We argue that it was the propagation and interconnection of the SLZs that promoted fracture nucleation due to very strong stress concentrations at their tips. According to the velocity-state frictional law (e.g., Dieterich, 1978, 1979; Ruina, 1983):

$$\mu = \mu_0 + (a-b)\ln(V/V_0)$$

where μ is the instantaneous friction coefficient, μ_0 is the steady-state coefficient of friction at a reference velocity V_0, V is the instantaneous sliding velocity, a and b are parameters that describe the initial response to the velocity change and the magnitude of the decay to the new steady-state value, respectively. If (a-b) > 0, velocity strengthening suppresses seismic activities. To the contrary, if (a-b) < 0, velocity weakening leads to unstable slip. Although the majority of deformation mechanisms in ductile shear zones, e.g., dislocation creep and diffusion creep, are velocity strengthening processes. Recent experimental studies and theoretical calculations have proved the occurrence of velocity weakening processes in an experimental deformation of a mixture of phyllosilicates and quartz grains. The results support the possibility of velocity weakening slip at the middle crust (e.g., Collettini et al., 2009, 2011; Den Hartog & Spiers, 2014; Niemeijer & Spiers, 2007). Furthermore, experimental studies on marble have also shown that dislocation and diffusion creep are, as strain rate increases, insufficient to accommodate large strain during GBS (e.g., Verberne et al., 2017). Intergranular mircopores are therefore generated and accompanied transition from steady-state flow to unstable slip. Experimental studies on interlayered quartz-biotite-quartz assemblies also exhibit stick-slip at 200-470 °C (e.g., Lu & He, 2014; Lu & He, 2018). The above discussions show that the compositions of SLZs in the present example are similar to those in the experimental studies. We would propose, hence, that SLZs from the natural shear zones may have the potential to trigger unstable slips or earthquakes at mid-crustal levels. A possible mechanism of seismic faulting may include the following processes: Stress concentrations at the tips of SLZs causes fracture nucleations. At the same time, the interconnection of SLZs will drive stress transfer, accompanying sudden decrease of rocks' strength and increase in slip velocity. Afterwards, velocity weakening processes within the SLZs enhance propagation of coseismic fracture and give rise to occurrence of earthquakes. The coseismic fractures are probably also the brittle precursors of ductile shear zones during subsequent deformation. On the debate of whether large earthquakes can be produced at the base of BDT, most previous studies suggest that the large earthquakes often occur at the top of BDT. It is generally suggested that there is not enough elastic energy to be stored in the ductile domain or at the base of BDT. The present study shows, however, that stress concentrations at fracture tips may overpass the rheological strength of rocks at the top of BDT domain. Besides, there is an obvious strength contrast between feldspar-framework and interconnected biotite-layers. Therefore, a lot of elastic energy will be stored in LBF, and release after the formation of IWP. It is thus expected that a marked strength decrease and strong elastic-energy release can be produced during the formation of strain localization zones, which may induce large earthquakes at the base of BDT.

6 conclusions

(1) The development of microcracks improve the porosity and permeability, and the generation of local low-pressure domains. Hence, microcracks drives fluids migration during initial

deformation periods. Creep cavitation becomes the dominant mechanism of fluid migration with grain-size reduction.

(2) The nucleation, propagation, and interconnection of microcracks at the tips of biotite grains, and the transition from LBF to IWP generate initial SLZs. The continuous occurrence of stage1-3 and relatively strain hardening of mature SLZs cause the widening of SLZs.

(3) The interconnection of SLZs leads to sudden decrease of rocks' strength and increase of strain rate, accompanying velocity weakening process and occurrence of earthquakes. Therefore, the SLZs are ductile precursors to earthquakes at the base of BDT.

Acknowledgments

The study is funded by the National Natural Science Foundation of China (41430211). We thank Xi Ma at the China Earthquake Administration for support during SEM and EBSD analysis. The EBSD date can be obtained via http://osf.io/5ang3/

References

Allen, J. L., (2005). A multi-kilometer pseudotachylyte system as an exhumed record of earthquake fracture geometry at hypocentral depths (Colorado, USA). Tectonophysics, 402(1-4), 0-54. http://doi.org/ 10.1016/j.tecto.2004.10.017

Bestmann, M., Pennacchioni, G., Nielsen, S., Göken, M., & Wall, H. D. (2012). Deformation and ultrafine dynamic recrystallization of quartz in pseudotachylyte-bearing brittle faults: a matter of a few seconds. Journal of Structural Geology, 38, 21-38. http://doi.org/10.1016/j.jsg.2011.10.001

Dell'Angelo, L. N., & Tullis, J. (1996). Textural and mechanical evolution with progressive strain in experimentally deformed aplite. Tectonophysics, 256(1-4), 0-82. http://doi.org/ 10.1016/0040-1951(95)00166-2

Den Hartog, S. A. M., Niemeijer, A. R., & Spiers, C. J. (2013). Friction on subduction megathrust faults: beyond the illite–muscovite transition. Earth and Planetary Science Letters, 373, 8-19. http://doi.org/10.1016/j.epsl.2013.04.036

Den Hartog, S. A. M., & Spiers, C. J. (2014). A microphysical model for fault gouge friction applied to subduction megathrusts. Journal of Geophysical Research: Solid Earth, 119(2), 1510-1529. http://doi.org/10.1002/2013JB01058

Chen, J., & C. J. Spiers (2016), Rate and state frictional and healing behavior of carbonate fault gouge explained using microphysical model, Journal of Geophysical Research: Solid Earth, 121, 8642–8665. http://doi.org/10.1002/2016JB013470

Chernak, L. J., Hirth, G., Selverstone, J., & Tullis, J. (2009). Effect of aqueous and carbonic fluids on the dislocation creep strength of quartz. Journal of Geophysical Research: Solid Earth, 114(B4). http://doi.org/10.1029/2008JB005884

Christiansen, P. P., & Pollard, D. D. (1997). Nucleation, growth and structural development of mylonitic shear zones in granitic rock. Journal of Structural Geology, 19(9), 1159-1172. http://doi.org/10.1016/S0191-8141(97)00025-4

Collettini, C., André Niemeijer, Viti, C., Smith, S. A. F., & Marone, C. (2011). Fault structure, frictional properties and mixed-mode fault slip behavior. Earth and Planetary Science Letters, 311(3-4), 0-327. http://doi.org/10.1016/j.epsl.2011.09.020

566 Czaplińska, Daria, Piazolo, S., & Zibra, I. (2015). The influence of phase and grain size
567 distribution on the dynamics of strain localization in polymineralic rocks. Journal of Structural
568 Geology, 72, 15-32. http://doi.org/10.1016/j.jsg.2015.01.001
569 Dieterich, J. H. (1978). Time-dependent friction and the mechanics of stick-slip. Pure and
570 Applied Geophysics, 116(4-5), 790-806. http://doi.org/10.1007/bf00876539
571 Dieterich, J. H. (1979). Modeling of rock friction: 1. experimental results and constitutive
572 equations. Journal of Geophysical Research Solid Earth, 84(B5), 2161-2168.
573 http://doi.org/10.1029/JB084iB05p02161
574 Ferrand, T. P., Hilairet, N., Incel, S., Deldicque, D., Labrousse, L., & Gasc, J., et al. (2017).
575 Dehydration-driven stress transfer triggers intermediate-depth earthquakes. Nature
576 Communications, 8, 15247. http://doi.org/10.1038/ncomms15247
577 Finch, M. A., Weinberg, R. F., & Hunter, N. J. R. (2016). Water loss and the origin of thick
578 ultramylonites. Geology, G37972.1. http://doi.org/10.1130/G37972.1
579 Fukuda, J., & Okudaira, T. (2013). Grain-size-sensitive creep of plagioclase accompanied by
580 solution–precipitation and mass transfer under mid-crustal conditions. Journal of Structural
581 Geology, 51(6), 61-73. http://doi.org/10.1016/j.jsg.2013.03.006
582 Fukuda, J. I., Okudaira, T., Satsukawa, T., & Michibayashi, K. (2012). Solution–precipitation of
583 k-feldspar in deformed granitoids and its relationship to the distribution of water.
584 Tectonophysics, 532-535, 175-185. http://doi.org/10.1016/j.tecto.2012.01.033
585 Fusseis, F., & Handy, M. R. (2008). Micromechanisms of shear zone propagation at the brittle–
586 viscous transition. Journal of Structural Geology, 30(10), 1242-1253.
587 http://doi.org/10.1016/j.jsg.2008.06.005
588 Fusseis, F., Regenauerlieb, K., Liu, J., Hough, R. M., & De, C. F. (2009). Creep cavitation can
589 establish a dynamic granular fluid pump in ductile shear zones. Nature, 459(7249), 974-977.
590 http://doi.org/10.1038/nature08051
591 Goncalves, C. C., Goncalves, L., & Hirth, G. (2015). The effects of quartz recrystallization and
592 reaction on weak phase interconnection, strain localization and evolution of microstructure.
593 Journal of Structural Geology, 71, 24-40. http://doi.org/ 10.1016/j.jsg.2014.11.010
594 Goncalves, P., Poilvet, J. C., Oliot, E., Trap, P., & Marquer, D. (2016). How does shear zone
595 nucleate? An example from the Suretta nappe (Swiss Eastern Alps). Journal of Structural
596 Geology, 86, 166-180. http://doi.org/10.1016/j.jsg.2016.02.015
597 Guermani, A., & Pennacchioni, G. (1998). Brittle precursors of plastic deformation in a granite:
598 An example from the Mont Blanc massif (Helvetic, western Alps). Journal of Structural
599 Geology, 20(2), 135-148. http://doi.org/10.1016/S0191-8141(97)00080-1
600 Gueydan, & Frédéric. (2003). Analysis of continental midcrustal strain localization induced by
601 microfracturing and reaction-softening. Journal of Geophysical Research, 108(B2), 2064.
602 http://doi.org/10.1029/2001JB000611
603 Haakon Fossen, Geane Carolina G. Cavalcante, Shear zones – A review, Earth-Science Reviews,
604 Volume 171, 2017, Pages 434-455, ISSN 0012-8252,
605 https://doi.org/10.1016/j.earscirev.2017.05.002.
606 Hirth, G., & Tullis, J. (1992). Dislocation creep regimes in quartz. Journal of Structural Geology,
607 14(2), 145-159. http://doi.org/10.1016/0191-8141(92)90053-Y
608 Hirth, G., & Tullis, J. (1994). The brittle-plastic transition in experimentally deformed quartz
609 aggregates. Journal of Geophysical Research, 99(B6), 11731.
610 http://doi.org/10.1029/93jb02873

611 Holyoke., C. W., & Tullis, J. (2006). Formation and maintenance of shear zones. Geology, 34(2),
612 105. http://doi.org/10.1130/g22116.1
613 Holyoke, C. W., & Tullis, J. (2006). The interaction between reaction and deformation: an
614 experimental study using a biotite + plagioclase + quartz gneiss. Journal of
615 Metamorphic Geology, 24(8), 743-762. http://doi.org/10.1111/j.1525-1314.2006.00666.x
616 Hobbs, B. E., & Ord, A. (1988). Plastic instabilities: implications for the origin of intermediate
617 and deep focus earthquakes. Journal of Geophysical Research, 93(B9), 10521.
618 http://doi.org/10.1029/jb093ib09p10521
619 Hobbs, B. E., Ord, A., & Teyssier, C. (1986). Earthquakes in the ductile regime? pure and
620 applied geophysics, 124(1-2), 309-336. http://doi.org/10.1007/BF00875730
621 Hunter, N. J. R., Pavlina Hasalová, Weinberg, R. F., & Wilson, C. J. L. (2015). Fabric controls
622 on strain accommodation in naturally deformed mylonites: the influence of interconnected
623 micaceous layers. Journal of Structural Geology, 83. http://doi.org/10.1016/j.jsg.2015.12.005
624 Ingles, J., Lamouroux, C., Soula, J. C., Guerrero, N., & Debat, P. (1999). Nucleation of ductile
625 shear zones in a granodiorite under greenschist facies conditions, Néouvielle massif, Pyrenees,
626 France. Journal of Structural Geology, 21(5), 555-576. http://doi.org/10.1016/S0191-
627 8141(99)00042-5
628 Ji, M., Liu, J. L., Hu, L., Shen, L., & Guan, H. (2015). Evolving magma sources during
629 continental lithospheric extension: Insights from the Liaonan metamorphic core complex,
630 eastern North China craton. Tectonophysics, 647, 48-62.
631 http://doi.org/10.1016/j.tecto.2015.01.023
632 Johnson, S. E., Vernon, R. H., & Upton, P. (2004). Foliation development and progressive strain-
633 rate partitioning in the crystallizing carapace of a tonalite pluton: microstructural evidence and
634 numerical modeling. Journal of Structural Geology, 26(10), 1845-1865.
635 http://doi.org/10.1016/j.jsg.2004.02.006
636 Kerrich, R., La Tour, T. E., & Barnett, R. L. (1981). Mineral reactions participating in
637 intragranular fracture propagation: implications for stress corrosion cracking. Journal of
638 Structural Geology, 3(1), 77-87. http://doi.org/10.1016/0191-8141(81)90058-4
639 Kirkpatrick, J. D., & Rowe, C. D. (2013). Disappearing ink: how pseudotachylytes are lost from
640 the rock record. Journal of Structural Geology, 52(5), 183-198.
641 http://doi.org/10.1016/j.jsg.2013.03.003
642 Kronenberg, A. K., Kirby, S. H., & Pinkston, J. (1990). Basal slip and mechanical anisotropy of
643 biotite. Journal of Geophysical Research: Solid Earth, 95. http://doi.org/10.1029/JB095iB12p
644 19257
645 Kruse, R., Holger Stünitz, & Kunze, K. (2001). Dynamic recrystallization processes in
646 plagioclase porphyroclasts. Journal of Structural Geology, 23(11), 1781-1802.
647 http://doi.org/10.1016/S0191-8141(01)00030-X
648 Lopez-Sanchez, M. A., & Llana-Fúnez, S. (2018). A cavitation-seal mechanism for ultramylonite
649 formation in quartzofeldspathic rocks within the semi-brittle field (Vivero fault, NW Spain).
650 Tectonophysics, 745, 132-153. http://doi.org/10.1016/j.tecto.2018.07.026.
651 Lin, A., Maruyama, T., Aaron, S., Michibayashi, K., Camacho, A., & Kano, K. I. (2005).
652 Propagation of seismic slip from brittle to ductile crust: evidence from pseudotachylyte of the
653 Woodroffe thrust, central Australia. Tectonophysics, 402(1-4), 0-35.
654 http://doi.org/10.1016/j.tecto.2004.10.016

Lin, A., Sun, Z., & Yang, Z. (2003). Multiple generations of pseudotachylyte in the brittle to ductile regimes, Qinling-Dabie Shan ultrahigh-pressure metamorphic complex, central China. Island Arc, 12(4), 423-435. http://doi.org/10.1046/j.1440-1738.2003.00407.x

Liu, J. L, Davis, G. A., Lin, Z., & Wu, F. (2005). The liaonan metamorphic core complex, Southeastern Liaoning Province, North China: a likely contributor to Cretaceous rotation of Eastern Liaoning, Korea and contiguous areas. Tectonophysics, 407(1-2), 0-80. http://doi.org/10.1016/j.tecto.2005.07.001

Liu, J. L., Gan, H., Jiang, H., & Zhang, J. (2016). Rheology of the middle crust under tectonic extension: Insights from the Jinzhou detachment fault zone of the Liaonan metamorphic core complex, eastern North China Craton. Journal of Asian Earth Sciences, S1367912016304266. http://doi.org/10.1016/j.jseaes.2016.12.024

Liu, J. L., Ji, M., Shen, L., Guan, H. M., & Davis, G. A. (2011). Early cretaceous extensional structures in the Liaodong peninsula: structural associations, geochronological constraints and regional tectonic implications. Science China, 54(6), 823-842. http://doi.org/CNKI:SUN:JDXG.0.2011-06-004

Liu, J. L., Shen, L., Ji, M., Guan, H., Zhang, Z., & Zhao, Z. (2013). The Liaonan/Wanfu metamorphic core complexes in the Liaodong peninsula: Two stages of exhumation and constraints on the destruction of the North China Craton. Tectonics, 32(5), 1121-1141. http://doi.org/10.1002/tect.20064

Liu, J. L., Walter, J. M., & Weber, K. (2002). Fluid-enhanced low-temperature plasticity of calcite marble: microstructures and mechanisms. Geology, 30(9), 787. http://doi.org/10.1130/0091-7613(2002)030<0787:feltpo>2.0.co;2

Lucas, S. B. (1990). Relations between thrust belt evolution, grain-scale deformation, and metamorphic processes: Cape Smith Belt, northern Canada. Tectonophysics, 178(2-4), 151-182. http://doi.org/10.1016/0040-1951(90)90144-w

Lu, Z., & He, C. (2014). Frictional behavior of simulated biotite fault gouge under hydrothermal conditions. Tectonophysics, 622, 62-80. http://doi.org/10.1016/j.tecto.2014.03.002

Lu, Z., & He, C. (2018). Friction of foliated fault gouge with a biotite interlayer at hydrothermal conditions. Tectonophysics, 740-741. http://doi.org/10.1016/j.tecto.2018.05.003

Mancktelow, N. S., & Pennacchioni, G. (2004). The influence of grain boundary fluids on the microstructure of quartz-feldspar mylonites. Journal of Structural Geology, 26(1), 47-69. http://doi.org/10.1016/S0191-8141(03)00081-6

Mclaren, A. C., & Pryer, L. L. (2001). Microstructural investigation of the interaction and interdependence of cataclastic and plastic mechanisms in feldspar crystals deformed in the semi-brittle field. Tectonophysics, 335(1), 1-15. http://doi.org/10.1016/S0040-1951(01)00042-7

Melosh, B. L., Rowe, C. D., Gerbi, C., Smit, L., & Macey, P. (2018). Seismic cycle feedbacks in a mid-crustal shear zone. Journal of Structural Geology, S0191814118301950. http://doi.org/10.1016/j.jsg.2018.04.004

Melosh, B. L., Rowe, C. D., Gerbi, C., Bate, C. E., & Shulman, D. (2016). The spin zone: transient mid-crust permeability caused by coseismic brecciation. Journal of Structural Geology, 87, 47-63. http://doi.org/10.1016/j.jsg.2016.04.003

Menegon, L., Pennacchioni, G., & H. Stünitz. (2006). Nucleation and growth of myrmekite during ductile shear deformation in metagranites. Journal of Metamorphic Geology, 24(7), 553-568. http://doi.org/10.1111/j.1525-1314.2006.00654.x

Moecher, D. P., & Steltenpohl, M. G. (2009). Direct calculation of fracture depth for an exhumed paleoseismogenic fault from mylonitic pseudotachylyte. Geology, 37(11), 999-1002. http://doi.org/10.1130/G30166A.1

Niemeijer, A. R., & Spiers, C. J. (2007). A microphysical model for strong velocity weakening in phyllosilicate-bearing fault gouges. Journal of Geophysical Research, 112(B10), B10405. http://doi.org/10.1029/2007JB005008

Nicolas, M., Hugues, R., Romain, A., Jacques, P., & Nicole, L. B. (2018). Large-scale strain localization induced by phase nucleation in mid-crustal granitoids of the south Armorican massif. Tectonophysics, 745, 46-65. https://doi.org/10.1016/j.tecto.2018.07.022.

Oliot, E., Goncalves, P.., Schulmann, K., Marquer, D., & Lexa, O. (2014). Mid-crustal shear zone formation in granitic rocks: constraints from quantitative textural and crystallographic preferred orientations analyses. Tectonophysics, 612-613, 63-80. http://doi.org/10.1016/j.tecto.2013.11.032

Pennacchioni, G. (2005). Control of the geometry of precursor brittle structures on the type of ductile shear zone in the Adamello tonalites, Southern Alps (Italy). Journal of Structural Geology, 27(4), 627-644. http://doi.org/10.1016/j.jsg.2004.11.008

Pennacchioni, G., & Mancktelow, N. S. (2007). Nucleation and initial growth of a shear zone network within compositionally and structurally heterogeneous granitoids under amphibolite facies conditions. Journal of Structural Geology, 29(11), 1757-1780. http://doi.org/10.1016/j.jsg.2007.06.002

Platt, J. P., & Behr, W. M. (2011). Grainsize evolution in ductile shear zones: implications for strain localization and the strength of the lithosphere. Journal of Structural Geology, 33(4), 537-550. http://doi.org/10.1016/j.jsg.2011.01.018

Price, N. A., Johnson, S. E., Gerbi, C. C., & West, D. P. (2012). Identifying deformed pseudotachylyte and its influence on the strength and evolution of a crustal shear zone at the base of the seismogenic zone. Tectonophysics, 518-521, 63-83. http://doi.org/10.1016/j.tecto.2011.11.011

Ruina, A. (1983). Slip instability and state variable friction laws. Journal of Geophysical Research Atmospheres, 881(B12), 10359-10370. http://doi.org/10.1029/JB088iB12p10359

Rowe, C. D., & Griffith, W. A. (2015). Do faults preserve a record of seismic slip: A second opinion. Journal of Structural Geology, 78, 1-26. http://doi.org/10.1016/j.jsg.2015.06.006

Kilian, R., Heilbronner, R., & Stünitz, H. (2011). Quartz grain size reduction in a granitoid rock and the transition from dislocation to diffusion creep. Journal of Structural Geology, 33(8), 1265-1284. http://doi.org/10.1016/j.jsg.2011.05.004

Segall, P., & Simpson, C. (1986). Nucleation of ductile shear zones on dilatant fractures. Geology, 14(14), 56-59. http://doi.org/10.1130/0091-7613(1986)14<56:NODSZO>2.0.CO;2

Shea, W. T., & Kronenberg, A. K. (1992). Rheology and deformation mechanisms of an isotropic mica schist. Journal of Geophysical Research Solid Earth, 97(B11). http://doi.org/10.1029/92JB00620

Sibson, R. H. (1980). Transient discontinuities in ductile shear zones. Journal of Structural Geology, 2(1), 165-171. http://doi.org/10.1016/0191-8141(80)90047-4

Sibson, R. H J., Moore, J. Mc., Rankin, A. H. (1975). Seismic pumping-a hydrothermal fluid transport mechanism. Journal of the Geological Society; 131 (6): 653–659. https://doi.org/10.1144/gsjgs.131.6.0653

744 Simpson, C., & Wintsch, R. P. (1989). Evidence for deformation-induced K-feldspar
745 replacement by myrmekite. Journal of Metamorphic Geology, 7(2), 261-275.
746 http://doi.org/10.1111/j.1525-1314.1989.tb00588.x
747 Stewart, C. A., & Miranda, E. A., (2017). The rheological evolution of brittle-ductile transition
748 rocks during the earthquake cycle: evidence for a ductile precursor to pseudotachylyte in an
749 extensional fault system, South Mountains, Arizona. Journal of Geophysical Research: Solid
750 Earth. http://doi.org/10.1002/2017JB014680
751 Stipp, M., Stünitz, H., Heilbronner, R., & Schmid, S. M. (2002). The eastern Tonale fault zone: a
752 'natural laboratory' for crystal plastic deformation of quartz over a temperature range from
753 250 to 700ºC. Journal of Structural Geology, 24(12), 1861-1884.
754 http://doi.org/10.1016/S0191-8141(02)00035-4
755 Takagi, H., Goto, K., & Shigematsu, N. (2000). Ultramylonite bands derived from cataclasite
756 and pseudotachylyte in granites, northeast Japan. Journal of Structural Geology, 22(9), 1325-
757 1339. http://doi.org/10.1016/S0191-8141(00)00034-1
758 Tullis, J., & Yund, R. A. (1985). Dynamic recrystallization of feldspar: a mechanism for ductile
759 shear zone formation. Geology, 13(4), 238-241. http://doi.org/10.1130/0091-
760 7613(1985)132.0.CO;2
761 Tullis, J., Yund, R., & Farver, J. (1996). Deformation-enhanced fluid distribution in feldspar
762 aggregates and implications for ductile shear zones. Geology, 24(1), 63.
763 http://doi.org/10.1130/0091-7613(1996)024<0063:DEFDIF>2.3.CO;2
764 Yang, J. H., Wu, F. Y., Chung, S. L., Lo, C. H., Wilde, S. A., & Davis, G. A. (2007). Rapid
765 exhumation and cooling of the liaonan metamorphic core complex: inferences from 40ar/39ar
766 thermochronology and implications for late Mesozoic extension in the eastern North China
767 Craton. Geological Society of America Bulletin, 119(11-12), 1405-1414.
768 http://doi.org/10.1130/B26085.1
769 Yund, R. A., & Snow, E. (1989). Effects of hydrogen fugacity and confining pressure on the
770 interdiffusion rate of NaSi-CaAl in plagioclase. Journal of Geophysical Research, 94(B8),
771 10662. http://doi.org/ 10.1029/jb094ib08p10662
772 Verberne, B. A., Chen, J., Niemeijer, A. R., De Bresser, J. H. P., Pennock, G. M., Drury, M. R.,
773 et al. (2017). Microscale cavitation as a mechanism for nucleating earthquakes at the base
774 of the seismogenic zone. Nature Communications, 8(1), 1645. http://doi.org/10.1038/s41467-
775 017-01843-3
776 Viegas, G., Menegon, L., & Archanjo, C. (2016). Brittle grain-size reduction of feldspar, phase
777 mixing and strain, localization in granitoids at mid-crustal conditions (Pernambuco shear zone,
778 NE Brazil). Solid Earth, 7(2), 375-396. http://doi.org/10.5194/se-7-375-2016
779 Weatherley, D. K., & Henley, R. W. (2013). Flash vaporization during earthquakes evidenced by
780 gold deposits. Nature Geoscience, 6(4), 294-298. http://doi.org/10.1038/NGEO1759
781 Wehrens, P., Baumberger, R., Berger, A., & Herwegh, M. (2016). How is strain localized in a
782 meta-granitoid, mid-crustal basement section? spatial distribution of deformation in the central
783 Aar massif (Switzerland). Journal of Structural Geology.
784 http://doi.org/10.1016/j.jsg.2016.11.004
785 Wehrens, P., Berger, A., Peters, M., Spillmann, T., & Herwegh, M. (2016). Deformation at the
786 frictional-viscous transition: evidence for cycles of fluid-assisted embrittlement and ductile
787 deformation in the granitoid crust. Tectonophysics. http://doi.org/10.1016/j.tecto.2016.10.022

White, W. C. (1996). Transient discontinuities revisited: pseudotachylyte, plastic instability and the influence of low pore fluid pressure on deformation processes in the mid-crust. Journal of Structural Geology, 18(12), 1471-1486. http://doi.org/10.1016/S0191-8141(96)00059-4

White, J. C. (2012). Paradoxical pseuditachylite-Fault melt outside the seismogenic zone. Journal of Structure Geology, 38, 11-20. http://doi.org/10.2016/j.jsg.2011.11.016

Whitmeyer, S. J., & Wintsch, R. P. (2005). Reaction localization and softening of texturally hardened mylonites in a reactivated fault zone, central argentina. Journal of Metamorphic Geology, 23(6), 411-424. http://doi.org/10.1111/j.1525-1314.2005.00588.x

Wibberley, C. (1999). Are feldspar-to-mica reactions necessarily reaction-softening processes in fault zones? Journal of Structural Geology, 21(8), 1219–1227. http://doi.org/10.1016/S0191-8141(99)00019-X

Wintsch, R. P., Christoffersen, R., & Kronenberg, A. K. (1995). Fluid-rock reaction weakening of fault zones. Journal of Geophysical Research, 100(B7), 13021. http://doi.org/10.1029/94jb02622

Wintsch, R. P., & Yeh, M. W. (2013). Oscillating brittle and viscous behavior through the earthquake cycle in the red river shear zone: monitoring flips between reaction and textural softening and hardening. Tectonophysics, 587, 46-62. http://doi.org/10.1016/j.tecto.2012.09.019